



Cite this: *Phys. Chem. Chem. Phys.*,
2020, 22, 21108

Understanding alkali metal cation affinities of multi-layer guanine quadruplex DNA[†]

C. Nieuwland, ^a F. Zaccaria ^a and C. Fonseca Guerra ^{*ab}

To gain better understanding of the stabilizing interactions between metal ions and DNA quadruplexes, dispersion-corrected density functional theory (DFT-D) based calculations were performed on double-, triple- and four-layer guanine tetrads interacting with alkali metal cations. All computations were performed in aqueous solution that mimics artificial supramolecular conditions where guanine bases assemble into stacked quartets as well as biological environments in which telomeric quadruplexes are formed. To facilitate the computations on these significant larger systems, optimization of the DFT description was performed first by evaluating the performance of partial reduced basis sets. Analysis of the stabilizing interactions between alkali cations and the DNA bases in double and triple-layer guanine quadruplex DNA reproduced the experimental affinity trend of the order $\text{Li}^+ < \text{Rb}^+ < \text{Na}^+ < \text{K}^+$. The desolvation and the size of alkali metal cations are thought to be responsible for the order of affinity. Nevertheless, for the alkali metal cation species individually, the magnitude of the bond energy stays equal for binding as first, second or third cation in double, triple and four-layer guanine quadruplexes, respectively. This is the result of an interplay between a decreasingly stabilizing interaction energy and increasingly stabilizing solvation effects, along the consecutive binding events. This diminished interaction energy is the result of destabilizing electrostatic repulsion between the hosted alkali metal cations. This work emphasizes the stabilizing effect of aqueous solvent on large highly charged biomolecules.

Received 26th June 2020,
Accepted 9th September 2020

DOI: 10.1039/d0cp03433a

rsc.li/pccp

1. Introduction

DNA sequences that are purine rich and contain runs of guanine (G) bases can form non-duplex four-stranded structures that are called guanine quadruplexes (GQs) (Fig. 1).^{1–5} GQs consist of stacked guanine quartets with alkali cations between the layers and occur in crucial regulatory regions of the human genome, such as telomeres and promoters. The guanine quartet (G_4) layers consists of four guanine bases assembled through Hoogsteen-type hydrogen bonding (Fig. 1a). The stabilization of GQ structures in telomeric regions has been shown to interfere with the activity of the enzyme telomerase, offering a tool to control the mechanism of elongation of telomeric ends that is related to cell senescence and therefore proliferation. On the other hand, the formation of GQ structures in telomeric and promoter regions of numerous genes can down-regulate transcription and suppress oncogene

expression. Therefore, GQs have been considered as an attractive target for anticancer drug design.^{6–9} This potential therapeutic application has led to a new field devoted to the design of (metallo)organic compounds that selectively interact, promote and stabilize the GQ folding.^{10–12}

However, in order to rationally design these so-called GQ-ligands, it is crucial to fully understand the physical principles behind the formation of GQs and the role of the alkali cations in the stabilization of these structures.

Previous work by Fonseca Guerra *et al.*^{13,14} has shown that the hydrogen bonding in G_4 relies on cooperativity. These synergistic effects originate from charge separation occurring upon hydrogen bonding, due to donor–acceptor interactions of the σ -electron system.¹⁵ It contradicts previous assumptions that the enhancement of the hydrogen bonds was solely caused by resonance of the π -electrons. In addition, Fonseca Guerra and co-workers demonstrated that although the presence of alkali metal cations between the G_4 layers weakens the hydrogen bonds, the synergy remains in telomeric structures.^{16–19}

The alkali metal cation that is located between two quartets was long believed to generate cation–dipole interactions with the eight interacting guanines and thereupon reducing the repulsion of the central oxygen atoms.^{20–22} This would enhance the hydrogen bonding strength and stabilize the GQ formation.

^a Department of Theoretical Chemistry and Amsterdam Center for Multiscale Modelling, AIMMS, Vrije Universiteit Amsterdam, De Boelelaan 1085 NL-1081HV Amsterdam, The Netherlands. E-mail: c.fonsecaguerra@vu.nl

^b Leiden Institute of Chemistry, Leiden University, Einsteinweg 55 NL-2333 CC Leiden, The Netherlands

[†] Electronic supplementary information (ESI) available. See DOI: 10.1039/d0cp03433a



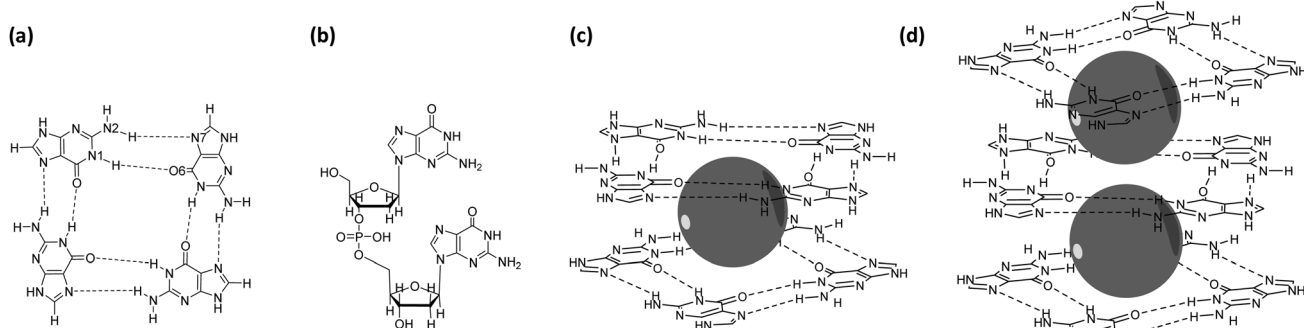


Fig. 1 Structural representation of (a) a guanine quartet (G_4) with inner ($N1(H) \cdots O6$) and outer ($N2(H) \cdots N7$) hydrogen bonds specified, (b) a guanine dimer (GG) with sugar-phosphate backbone neutralized with H^+ as counterion, (c) a guanine quadruplex double-layer scaffold with an alkali metal ion presented as a grey sphere ($G_4 - M^+ - G_4$) and (d) a guanine quadruplex triple-layer scaffold with two alkali metal ions ($G_4 - M^+ - G_4 - M^+ - G_4$).

This idea was rationalized by the presence of significant negative charge located at the central cavity of the G_4 .²¹ In 2016, work by Zaccaria *et al.*²³ revealed that the central cation is not needed to reduce repulsion between the oxygen atoms, but rather provides additional stability of the quadruplex by electrostatic and donor–acceptor interactions between the oxygens and the cation. Later work showed that inclusion of the metal cation into the quadruplex significantly lowers the Gibbs free energy of formation of the cationic species compared to the formation of the empty scaffold.²⁴ This led to the insight that the actual need for the cation is to overcome the entropic penalty.

Guanine quadruplexes can host different alkali metal cations, and many experimental studies have revealed an overall affinity sequence of $K^+ > Na^+, Rb^+ \gg Li^+, Cs^+$ in water.^{25–27} Research has been devoted to finding an explanation of this affinity trend.^{28–30} Williamson *et al.*²⁸ suggested in 1989 that the overserved ion specificity was related to the *snug fit* of the alkali cations into the cavity of the quadruplex, thus the size of the cations. Later, Hud and co-workers³⁰ claimed that the Gibbs free energy of solvation of the alkali metal cations was the determining factor, since cations have to be desolvated completely before they can access the inner channel of GQs. This idea was supported by the theoretical work of Gu and Leszczynski.²⁹

Zaccaria *et al.*²³ showed that both the ionic radius, as well as the Gibbs free energy of solvation, are of equal importance in determining the order of cation affinity in GQ structures. These results were obtained from extensive computational analysis of the electronic properties of double-layer GQ structures interacting with the different alkali metal cations. These computations were based on dispersion-corrected density functional theory (DFT-D).^{31–36} The study of Zaccaria and co-workers involved double-layer quadruplexes (Fig. 1c). However, natural occurring GQ structures can be encountered as multiple stacks of G_4 .^{4,7,37} Therefore, we have investigated if our previous results and conclusions can be extended to larger systems which include interactions between adjacent cations.

In this work we investigate the electronic interactions of double, triple and four-layer GQ structures (with and without sugar-phosphate backbone) with the different alkali metal

cations in aqueous solution by computational analysis using DFT-D based calculations. To facilitate the computations on these significant larger systems, optimization of the DFT description was performed at first by evaluating the performance of partial reduced basis sets. In case of the triple-layer systems, the computational geometries involve quadruplex structures occupied by one potassium cation, to which a second alkali metal cation is introduced. The four-layer GQ comprises a structure hosting three potassium cations. The calculations simulate the situation of quadruplexes under supramolecular and biological conditions in aqueous solution.

2. Computational methods

2.1 General procedure

All the calculations were performed using the Amsterdam Density Functional (ADF) program (ADF2017.103).^{38–40} Geometry optimizations and stationary point energy calculations were based on dispersion-corrected relativistic density functional theory at the ZORA-BLYP-D3(BJ) level of theory.^{31–36,41} A TZP basis set was used for the description of the alkali metal cations and the guanine bases, whereas DZ was used as basis set for the sugar phosphate backbone. Our benchmark study revealed that the usage of these smaller basis sets is justified (see Section 3.1 and ESI† Fig. S1 and S2). The use of the BLYP exchange functional in combination with D3 London dispersion correction with Becke–Johnson damping is supported by previous computational work on guanine quadruplexes that demonstrated that this description results in reliable geometries and trends in line with experiment.^{23,24,35,42} In addition, Sedlak *et al.* showed that BLYP-D3(BJ) outperforms semi-empirical functionals, such as M06-2X, in terms of accuracy: cost ratio for the description of non-covalent interactions.⁴³ Because of this combination of high accuracy and low computational costs, BLYP-D3(BJ) was used in this work.

No geometrical constraints were imposed on the optimized geometries. This also applied to the guanine quadruplexes without backbone (129 atoms (2-layer), 194 atoms (3-layer) and 259 atoms (4-layer)) and the guanine quadruplex with



backbone (265 atoms (2-layer) and 402 atoms (3-layer)). The guanine quadruplexes in this work are parallel stranded right-handed GQ structures with anti-glycosidic torsion angles at all guanines. Biological GQ structures are also constituted by loop regions with dangling nucleobases. However, dangling nucleobases do not have significant influence on binding properties of the shielded interior of the quadruplex and are therefore omitted in the model systems.

Optimized geometries of the double-layer GQ structures at the ZORA-BLYP-D3 (BJ)/TZ2P level of theory of Zaccaria *et al.* were used as starting point for the calculations of the triple-layer systems.^{23,24} Solvent effects in water have been taken into account with the conductor-like screening model (COSMO), as implemented in the ADF program.^{36,44–46} Radii of the cations have been determined by reproduction of the solvation energy of the cation according to the procedure presented in ref. 36 (see ESI,† Table S1). In ADF releases after ADF2016 an improved method to construct the solvation surface in COSMO (Delley cavity construction instead of the Solvent-Excluding-Surface (SES) method) was implemented that led to more reliable geometry optimizations when using the COSMO solvation model.⁴⁰ To compare the results of the double-layer quadruplexes with the triple-layer systems, the results of Zaccaria *et al.* were reproduced using the improved solvation model. Energies regarding the double-layer GQs were calculated as formulated by Zaccaria and co-workers.²³

The energy of formation, ΔE_{form} , of the triple-layer guanine quadruplex structures is defined by eqn (1a) and (1b), for the GQ without and with sugar-phosphate backbone, respectively (see also Fig. 2).

$$\Delta E_{\text{form}} = E(\text{G}_4\text{--K}^+\text{--G}_4\text{--M}^+\text{--G}_4) - 12 \cdot E(\text{G}) - E(\text{K}^+) - E(\text{M}^+) \quad (1\text{a})$$

$$\Delta E_{\text{form}} = E(\text{GQ--K}^+\text{--M}^+) - 4 \cdot E(\text{GGG}) - E(\text{K}^+) - E(\text{M}^+) \quad (1\text{b})$$

$E(\text{G})$ is the energy of the separately optimized geometry of the guanine monomer. $E(\text{GGG})$ refers to the energy of the

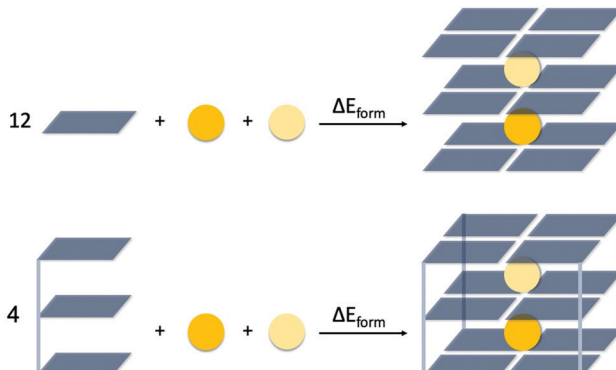


Fig. 2 Definition of the formation energy (ΔE_{form}) of the triple-layer guanine quadruplex structures without (G_4 , top scheme) and with sugar-phosphate backbone (GQ, bottom scheme).

optimized guanosine trimer, wherein the sugar-phosphate backbone is neutralized by H^+ as counterion (Fig. 1b). Zaccaria *et al.* found that neutralization with H^+ gives the same affinity trend as with neutralization with Na^+ .²³ $E(\text{M}^+)$ denotes the energy of the central alkali metal cation (*i.e.* Li^+ , Na^+ , K^+ or Rb^+). $E(\text{G}_4\text{--K}^+\text{--G}_4\text{--M}^+\text{--G}_4)$ and $E(\text{GQ--K}^+\text{--M}^+)$ are the energies of the triple-layer GQs, without and with backbone, in the optimal geometry.

2.2 Bond energy analysis

The bond energy between the second alkali metal cation and the triple-layer GQ structures, with one cavity occupied by K^+ and one empty cavity, is formulated by eqn (2a) and (2b) for the guanine quadruplexes without (G_4) and with backbone (GQ), respectively (see also Fig. 3).

$$\Delta E_{\text{bond}} = E(\text{G}_4\text{--K}^+\text{--G}_4\text{--M}^+\text{--G}_4)_{\text{aq}} - E(\text{G}_4\text{--K}^+\text{--G}_4\text{--[]--G}_4)_{\text{aq}} - E(\text{M}^+)_{\text{aq}} \quad (2\text{a})$$

$$\Delta E_{\text{bond}} = E(\text{GQ--K}^+\text{--M}^+)_{\text{aq}} - E(\text{GQ--K}^+\text{--[]})_{\text{aq}} - E(\text{M}^+)_{\text{aq}} \quad (2\text{b})$$

In these equations $E(\text{G}_4\text{--K}^+\text{--G}_4\text{--M}^+\text{--G}_4)_{\text{aq}}$ and $E(\text{GQ--K}^+\text{--M}^+)_{\text{aq}}$ are the energies of the in water optimized triple-layer GQs, without and with backbone, occupied by one potassium cation and another alkali metal cation ($\text{M}^+ = \text{Li}^+$, Na^+ , K^+ or Rb^+). $E(\text{G}_4\text{--K}^+\text{--G}_4\text{--[]--G}_4)_{\text{aq}}$ and $E(\text{GQ--K}^+\text{--[]})_{\text{aq}}$ denote the energies of the optimized triple-layer GQs in water, without and with backbone, occupied by one potassium cation.

In order to understand the different components that determine the trend in bond energy (*i.e.* cation affinity) the bond energy was partitioned as formulated by eqn (3) (see also Fig. 3).

$$\Delta E_{\text{bond}} = \Delta E_{\text{desolv}} + \Delta E_{\text{prep}} + \Delta E_{\text{int}} + \Delta E_{\text{solv}} \quad (3)$$

The desolvation (ΔE_{desolv}) and solvation energy (ΔE_{solv}) can be computed by taking the energy difference between the solvated structure and the gas phase single-point calculation of the solvated optimized geometry (see eqn (4) and (5)). The subscript 'aq' indicates calculations performed with COSMO, whereas the subscript 'gas' refers to gas phase calculations.

$$\Delta E_{\text{desolv}} = E(\text{G}_4\text{--K}^+\text{--G}_4\text{--[]--G}_4)_{\text{gas}} - E(\text{G}_4\text{--K}^+\text{--G}_4\text{--[]--G}_4)_{\text{aq}} + E(\text{M}^+)_{\text{gas}} - E(\text{M}^+)_{\text{aq}} \quad (4\text{a})$$

$$\Delta E_{\text{desolv}} = E(\text{GQ--K}^+\text{--[]})_{\text{gas}} - E(\text{GQ--K}^+\text{--[]})_{\text{aq}} + E(\text{M}^+)_{\text{gas}} - E(\text{M}^+)_{\text{aq}} \quad (4\text{b})$$

$$\Delta E_{\text{solv}} = E(\text{G}_4\text{--K}^+\text{--G}_4\text{--M}^+\text{--G}_4)_{\text{aq}} - E(\text{G}_4\text{--K}^+\text{--G}_4\text{--M}^+\text{--G}_4)_{\text{gas}} \quad (5\text{a})$$

$$\Delta E_{\text{solv}} = E(\text{GQ--K}^+\text{--M}^+)_{\text{aq}} - E(\text{GQ--K}^+\text{--M}^+)_{\text{gas}} \quad (5\text{b})$$

The preparation energy (ΔE_{prep}) is the energy required to deform the solvated state geometry of the triple-layer GQ structure, with one cavity occupied by K^+ and one empty cavity, ($\text{G}_4\text{--K}^+\text{--G}_4\text{--[]--G}_4$ or $\text{GQ--K}^+\text{--[]}$) to the geometry it acquires when it interacts with the second alkali metal cation, but calculated in the gas phase (see Fig. 3). The values of the preparation have been checked to be almost phase independent



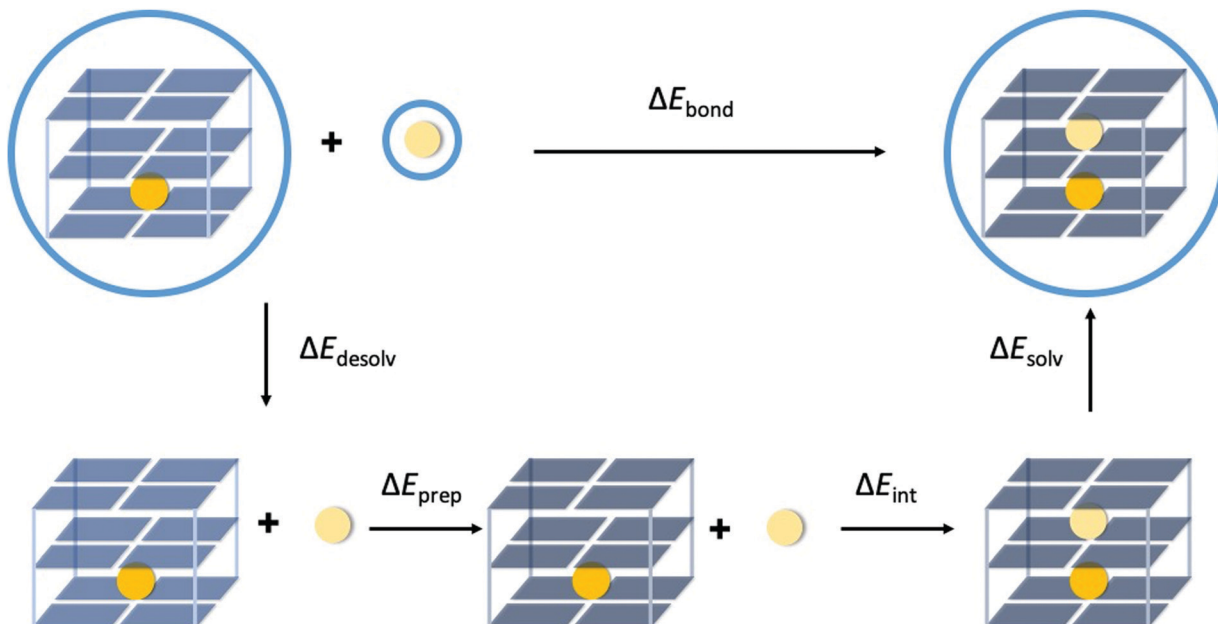


Fig. 3 Partitioning of the bond energy between the second alkali metal cation (light yellow sphere) in the empty cavity of the by K⁺ (orange sphere) occupied triple-layer guanine quadruplex structure. The blue circles surrounding the structures indicate that the calculation is performed with COSMO to simulate water.

(see ESI,† Table S2). The procedure to determine ΔE_{prep} in the gas phase has been chosen to not have contributions by the implicit solvent in this energy term.

Finally, the interaction energy (ΔE_{int}) can be computed in the gas phase for the geometries of the solvated state (eqn (6a) and (6b)).

$$\Delta E_{\text{int}} = E(\text{G}_4\text{--K}^+\text{--G}_4\text{--M}^+\text{--G}_4)_{\text{gas}} - E(\text{G}_4\text{--K}^+\text{--G}_4\text{--[]--G}_4)_{\text{gas}} - E(\text{M}^+)_{\text{gas}} \quad (6a)$$

$$\Delta E_{\text{int}} = E(\text{GQ--K}^+\text{--M}^+)_{\text{gas}} - E(\text{GQ--K}^+\text{--[]})_{\text{gas}} - E(\text{M}^+)_{\text{gas}} \quad (6b)$$

This approximation can be made since the interaction of the alkali metal cation occurs on the interior of the quadruplex cavity, which is shielded from the solvent by the guanine bases and sugar-phosphate backbone. In addition, it is assumed that the negatively charged central cavity prevents entering of water molecules.¹

The interaction energy is further decomposed based on the Kohn–Sham molecular orbital theory using a quantitative energy decomposition analysis (EDA), which divides the total interaction energy (ΔE_{int}) into electrostatic interaction (ΔV_{elstat}), Pauli repulsion (ΔE_{Pauli}), orbital interaction (ΔE_{oi}) and dispersion correction (ΔE_{disp}) components (eqn (7)).⁴⁷

$$\Delta E_{\text{int}} = \Delta V_{\text{elstat}} + \Delta E_{\text{Pauli}} + \Delta E_{\text{oi}} + \Delta E_{\text{disp}} \quad (7)$$

ΔV_{elstat} corresponds to the classical electrostatic interactions between the unperturbed charge distributions of the prepared (*i.e.* deformed) interacting molecular fragments and is usually attractive. ΔE_{Pauli} comprises the destabilizing interactions between the occupied orbitals and accounts for any steric repulsion. The term ΔE_{oi} includes charge transfer (*i.e.* donor–acceptor

interactions between occupied orbitals on one of the interacting fragments and unoccupied orbitals on the other, including the HOMO–LUMO interactions) and polarization (empty-occupied orbital mixing on one fragment due to the presence of the other fragment). The term ΔE_{disp} includes dispersion corrections.

2.3 Voronoi deformation density analysis

The Voronoi deformation density (VDD) method allows analysis of the electronic redistributions within polyatomic fragments when a chemical bond is formed between these molecular fragments.^{48,49} The VDD atomic charges (ΔQ_{M⁺}) have been calculated for the second alkali metal cations in the central cavity of the triple-layer quadruplex (GQ–K⁺–M⁺). ΔQ_{M⁺} is computed as the (numerical) integral of the deformation density (Δρ(**r**)) in the volume of the Voronoi cell of cation M⁺ associated with the formation of the triple-layer quadruplex from the quadruplex hosting one K⁺ and the second metal cation (see eqn (8)). The Voronoi cell of M⁺ is the space defined by the bond midplanes on and perpendicular to all bond axes between nucleus M⁺ and its neighbouring nuclei.

$$\Delta Q_{\text{M}^+} = - \int_{\text{Cell}} \times \left(\rho_{\text{GQ--K}^+\text{--M}^+}(\mathbf{r}) - \rho_{\text{GQ--K}^+\text{--[]}}(\mathbf{r}) - \rho_{\text{M}^+}(\mathbf{r}) \right) \text{d}\mathbf{r} \quad (8)$$

ΔQ_{M⁺} is an indication for the number of electrons that flows into (ΔQ_{M⁺} < 0) or out of (ΔQ_{M⁺} > 0) the Voronoi cell of M⁺ as result of the interaction of M⁺ with GQ–K⁺–M⁺. Cell is the Voronoi Cell of M⁺ in GQ–K⁺–M⁺.

3. Results and discussion

3.1 Basis set dependency

Since DNA-based systems, especially including metals, encounter many non-covalent interactions, the use of triple-zeta (or larger) basis sets is often recommended when studying these systems.⁵⁰ However, in these large (supramolecular) biomolecules, large basis sets can make the calculations too expensive. Therefore, smaller basis sets, which would combine high computational speed and accuracy, are preferred. The performance of the basis sets SZ, DZ, DZP, TZP and TZ2P and combinations of these for different regions of the quadruplexes were screened by stationary point calculations on the optimized double-layer GQ geometries at the ZORA-BLYP-D3(BJ)/TZ2P level of theory of Zaccaria *et al.* (see ESI† Fig. S1 and S2).²³ By comparing the obtained energies with the energy of the TZ2P calculation, the most promising (*i.e.* lowest computational cost, with sufficient accuracy (≤ 1 kcal mol⁻¹ deviation)) basis set combination was selected. The results show that usage of different basis sets within the ring system of the guanine base, leads to significant errors in calculated energies (ESI,† Fig. S1). This result is in accordance to the results found by Fonseca Guerra *et al.* in 1999.⁵¹ In this work it was found that hydrogen bonding is not a local effect, but affects the distributions of the σ and π electrons throughout the whole DNA base. The results of this work show that the basis set combination using TZP for the guanine bases and K⁺, in combination with a DZ basis set for the sugar-phosphate backbone gives a ΔE_{form} within the 1 kcal mol⁻¹ deviation range and seems to be sufficient to describe quadruplexes (Table 1 and ESI,† Fig. S2). To validate this, the performance of the TZP/DZ basis set combination was examined in a geometry optimization of GQ-K⁺. The results of these calculations are depicted in Table 1. Both the energy and the geometrical parameters are in good accordance with the by TZ2P obtained results. Nevertheless, the average calculation time per cycle is almost three times shorter. Therefore, using the TZP/DZ basis set combination is likely to significantly reduce the calculation time on DNA based systems, compared to the conventional TZ2P basis set, while maintaining the required computational accuracy. The TZP/DZ basis set combination was used in the calculations of the quadruplexes throughout this work.

3.2 Structure and energy of formation

Previous results by Zaccaria *et al.* showed that the double-layer quadruplexes preferably facilitate the hosting of K⁺ and that the order of affinity can be explained by the size of the alkali metal cation and the desolvation energy.²³ Because of improvement of the implicit solvation model in the newer ADF version, the energies and structures of the double-layer GQs were recalculated in this work.⁴⁰ To study the interaction between a second alkali metal cations in the by one K⁺ occupied triple-layer guanine quadruplex, two additional model systems have been studied computationally: G₄-K⁺-G₄-M⁺-G₄ and GQ-K⁺-M⁺ (see Fig. 1 and Fig. 4). The latter system also includes the sugar-phosphate backbone which is neutralized by H⁺ as counterion.^{23,50} The

Table 1 Performance of DFT-D ZORA-BLYP-D3(BJ)/TZP/DZ in the geometry optimization of GQ-K⁺ in the gas phase

	TZ2P	TZP/DZ
Calculated ΔE_{form}^a	-277.3	-277.0
Relative average calculation time/geometry optimization cycle	1	0.3
$d[\text{O}-\text{K}^+]^b$	2.81	2.81
R^c	3.12	3.11
N2(H)···N7 ^d	2.90	2.90
N1(H)···O6 ^e	2.81	2.80
$\angle \text{OPO}^f$	107.0	106.1

^a The energies (in kcal mol⁻¹) were computed with the DFT-D method at the ZORA-BLYP-D3(BJ) level of theory in the gas phase. ^b Average distance (in Å) between the oxygen atoms and the midpoint of the eight oxygen atoms. ^c Difference in the average z-coordinate (in Å) of the upper and lower oxygen atoms. ^d Average outer hydrogen bond distance N2(H)···N7 (in Å). ^e Average inner hydrogen bond dissonance N1(H)···O6 (in Å). ^f Average OPO angle (in degrees) of bridging two sugar molecules of the backbone.

energy of formation (ΔE_{form} , eqn (1)) and geometrical parameters of the double and triple-layer GQs are listed in Table 2. The most stable complexes (*i.e.* most negative ΔE_{form}) are the quadruplexes facilitating only K⁺. For example, the GQ-K⁺-M⁺ system with M⁺ = K⁺ is most stable, followed by Na⁺ (+2.2 kcal mol⁻¹), Rb⁺ (+4 kcal mol⁻¹) and Li⁺ (+13 kcal mol⁻¹). These results are consistent with experimental findings^{25–27} and the computational results found by Zaccaria *et al.*²³ for the double-layer quadruplexes. Thus, from Table 2 it can be concluded that also for the triple-layer quadruplexes, the trend in affinity follows the order K⁺ > Na⁺ > Rb⁺ > Li⁺. Although, improvement of the computational order of affinity is obtained by the more realistic system with backbone, the same trend was found for the simplified quadruplexes without backbone (G₄), but with smaller energy differences for the different cations. This justifies the usage of quadruplex systems without backbone for the study of cation-quadruplex interactions. This, together with the reduced computational costs, by using a smaller basis set (see Section 3.1 and ESI,† Fig. S2 and Table 1), opens up possibilities to study larger multi-layer systems. It should be noted that for the G₄-K⁺-G₄-M⁺-G₄ system, the order of Na⁺ and K⁺ is reversed by a small energy difference of 0.5 kcal mol⁻¹. Since the experimental energy difference for Na⁺ and K⁺ is only a few kcal mol⁻¹, small deviations in geometry due to the lack of the rigidity of the backbone, can already reverse the trend.²⁷ The computed values of the distance between the metal cation (M⁺) and the surrounding oxygen atoms ($d[\text{O}-\text{M}^+]$) are close to the experimental values^{29,30,52} and the values computed for the double-layered systems.²³ Also, the average distance (R) between the upper and lower oxygen atoms and the hydrogen bond distances do not change significantly upon introduction of a third guanine layer.

3.3 Partitioning of the bond energy

In order to explain the computed trends in cation affinity for the triple-layer systems and identify differences compared to the double-layers GQs, the bond energy (ΔE_{bond}) was partitioned into different terms (see eqn (3)). Solvation effects that



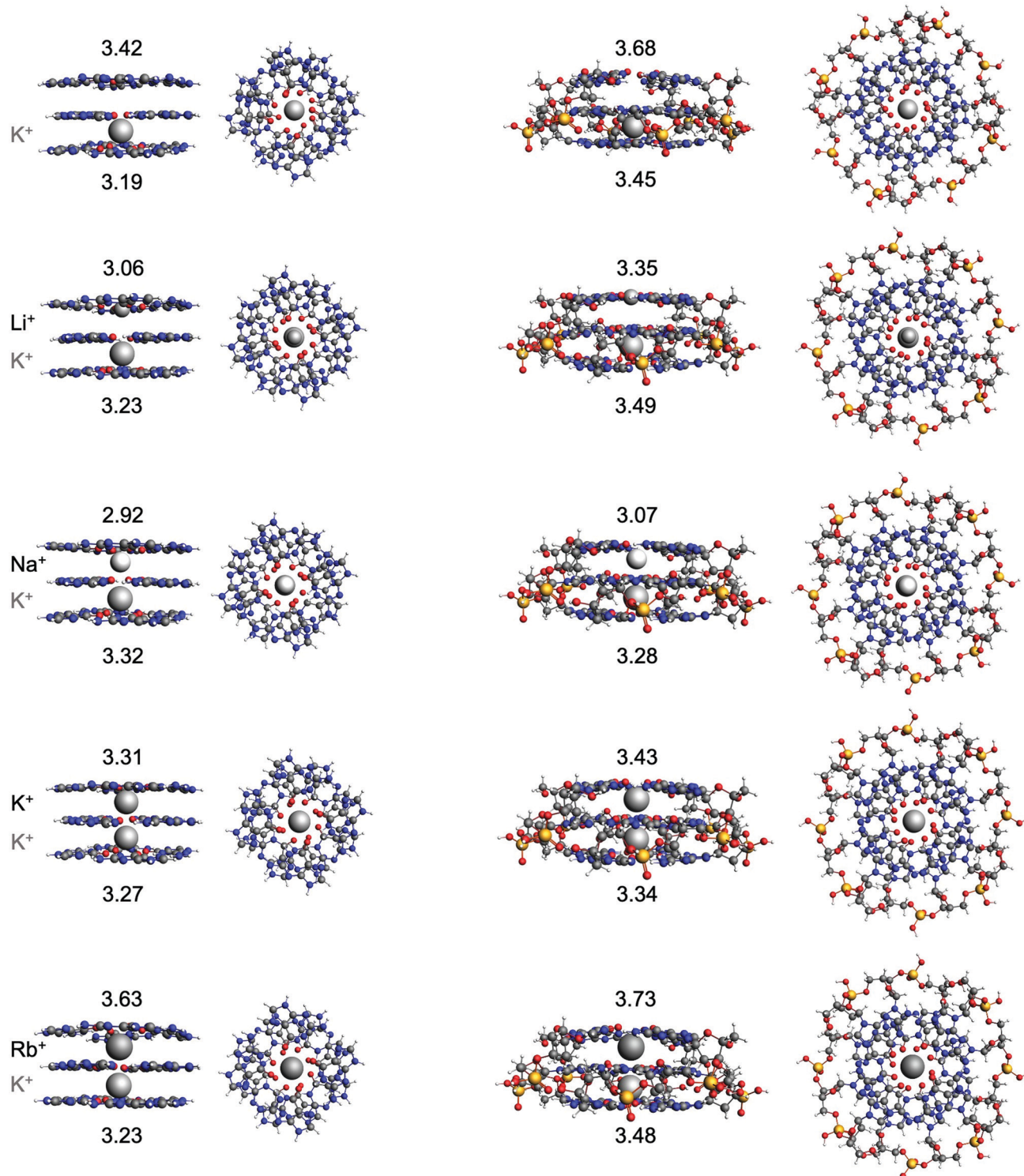


Fig. 4 Structures of $\text{G}_4\text{--K}^+\text{--G}_4\text{--[]--G}_4$, $\text{G}_4\text{--K}^+\text{--G}_4\text{--M}^+\text{--G}_4$, $\text{GQ}\text{--K}^+\text{--[]}$ and $\text{GQ}\text{--K}^+\text{--M}^+$ where M^+ is an alkali metal cation. The G_4 structures were optimized at the ZORA-BLYP-D3(BJ)/TZP level of theory and the GQ structures at the ZORA-BLYP-D3(BJ)/TZP/DZ level of theory with COSMO to simulate water. The difference in the average z-coordinate of the upper and lower oxygen atoms (R , in Å), as measure for the interplanar distance of adjacent guanine quartets, is displayed.

may contribute to the observed trend can be studied computationally by the terms ΔE_{desolv} and ΔE_{solv} (eqn (4) and (5)). Furthermore, the effect of the size of the second alkali cation can be determined

by the preparation energy term (ΔE_{prep} , eqn (3)) and stabilizing interactions between the cation and the quadruplex scaffold by the interaction energy (ΔE_{int} , eqn (6) and (7)). The preparation energy

Table 2 Energies of formation^a (in kcal mol⁻¹) of the double- and triple-layer guanine quadruplexes and geometrical parameters (in Å) of the layer hosting M⁺. The geometrical parameters of the layer hosting K⁺ are shown in parentheses in case of the triple-layer systems

System	M ⁺	d[O-M ⁺] ^b	R ^c	N2(H)···N7 ^d	N1(H)···O6 ^e	ΔE _{form} ^a
G ₄ -M ⁺ -G ₄	No metal	2.86	3.35	2.88	2.80	-102.4
	Li ⁺	2.14	3.10	—	—	-128.2
	Na ⁺	2.68	2.90	2.85	2.81	-144.1
	K ⁺	2.81	3.23	2.88	2.82	-144.3
	Rb ⁺	2.94	3.56	2.90	2.83	-137.7
GQ-M ⁺	No metal	2.92	3.57	2.89	2.81	-83.2
	Li ⁺	2.12	3.41	—	—	-109.3
	Na ⁺	2.70	3.01	2.86	2.81	-122.6
	K ⁺	2.84	3.36	2.89	2.83	-123.9
	Rb ⁺	2.95	3.65	2.90	2.84	-118.1
G ₄ -K ⁺ -G ₄ -M ⁺ -G ₄	No metal	2.88 (2.80)	3.42 (3.19)	2.87 (2.87)	2.80 (2.81)	-212.3
	Li ⁺	2.14 (2.81)	3.06 (3.23)	—	—	-241.4
	Na ⁺	2.67 (2.81)	2.92 (3.32)	2.83 (2.85)	2.81 (2.82)	-255.8
	K ⁺	2.82 (2.81)	3.31 (3.27)	2.85 (2.87)	2.82 (2.83)	-255.3
	Rb ⁺	2.94 (2.81)	3.63 (3.23)	2.86 (2.88)	2.83 (2.83)	-247.2
GQ-K ⁺ -M ⁺	No metal	2.96 (2.84)	3.68 (3.45)	2.87 (2.86)	2.81 (2.79)	-205.9
	Li ⁺	2.14 (2.84)	3.35 (3.49)	—	—	-229.7
	Na ⁺	2.71 (2.85)	3.07 (3.28)	2.83 (2.84)	2.80 (2.80)	-242.8
	K ⁺	2.86 (2.86)	3.43 (3.34)	2.86 (2.86)	2.82 (2.80)	-245.0
	Rb ⁺	2.97 (2.90)	3.73 (3.48)	2.88 (2.87)	2.84 (2.78)	-238.8

^a All energies (in kcal mol⁻¹) were computed with the DFT-D method at the ZORA-BLYP-D3(BJ)/TZP(DZ) level of theory with COSMO to simulate water.

^b Average distance (in Å) between the oxygen atoms and the second alkali metal cation. For the empty cavities the midpoint of the eight adjacent oxygen atoms was taken. In the case of Li⁺ the average distance to the oxygen atoms is taken of the quartet where Li⁺ lies in the center. ^c Difference in the average z-coordinate (in Å) of the upper and lower oxygen atoms. ^d Average outer hydrogen bond distance N2(H)···N7 (in Å). This value is not presented in the case of Li⁺, since Li⁺ lies in the center of one of the quartets. ^e Average inner hydrogen bond dissonance N1(H)···O6 (in Å).

(i.e. deformation of the quadruplex scaffold to facilitate the second alkali cation) is expected to be smaller when the alkali cation fits well into the central cavity of the scaffold. The interaction energy is likely to be larger for cations with more favourable coordination to the negatively charged oxygen atoms. The partitioning of the bond energy is presented in Table 3 and graphically presented for the quadruplexes with backbone (GQ) in Fig. 5. In Fig. 5 the solid lines represent the results found in this study for the three-layer quadruplex systems, whereas the dashed lines represent the results found for the double-layered quadruplexes.

In all cases, the bond energy is mainly the sum of a strong interaction energy, compensated by a large desolvation energy. The preparation energy does not vary much for the different

cations and decreases upon increasing the size of the cation. This trend can be explained by looking at the cation–oxygen distance (d[O-M⁺]) and interplanar distance (R) (Table 2) that determine the size of the cavity hosting the second cation. The values of the geometrical parameters d[O-M⁺] and R come closer to the values of the empty cavity going from Li⁺ to Rb⁺. For the guanine bases to interact with the smaller cations (Li⁺ and Na⁺), the cavity should shrink. This leads to a higher preparation energy than in the case of the larger cations (K⁺ and Rb⁺), which give rise to less distortion of the empty cavity.

To investigate the contributions of geometrical effects and solvation effects, the sum of the interaction and preparation energy ($\Delta E_{\text{int}} + \Delta E_{\text{prep}}$) is displayed in Table 3, as well as the sum of the solvation and desolvation energy ($\Delta E_{\text{desolv}} + \Delta E_{\text{solv}}$),

Table 3 Partitioning of the bond energy (in kcal mol⁻¹) of alkali metal cations (M⁺) with G₄-[-]-G₄, GQ-[-], G₄-K⁺-G₄-[-]-G₄ and GQ-K⁺-[-]^a

System	M ⁺	ΔE _{bond}	ΔE _{desolv}	ΔE _{prep}	ΔE _{int}	ΔE _{solv}	ΔE _{desolv} + ΔE _{solv}	ΔE _{prep} + ΔE _{int}
G ₄ -M ⁺ -G ₄	Li ⁺	-25.8	208.1	10.4	-159.4	-85.0	123.1	-149.0
	Na ⁺	-41.8	182.1	8.0	-149.9	-81.9	100.2	-141.9
	K ⁺	-41.9	164.4	3.3	-126.9	-82.7	81.7	-123.6
	Rb ⁺	-35.3	160.3	2.6	-114.2	-84.1	76.2	-111.5
	Li ⁺	-26.1	286.2	9.4	-163.6	-158.2	128.0	-154.2
GQ-M ⁺	Na ⁺	-39.5	260.2	8.4	-154.2	-153.8	106.4	-145.8
	K ⁺	-40.7	242.5	4.0	-133.0	-154.2	88.3	-129.0
	Rb ⁺	-34.9	238.4	3.0	-121.3	-155.0	83.4	-118.3
	Li ⁺	-29.1	235.4	9.6	-119.1	-155.0	80.4	-109.5
	Na ⁺	-43.4	209.4	8.4	-105.1	-156.1	53.3	-96.7
G ₄ -K ⁺ -G ₄ -M ⁺ -G ₄	K ⁺	-42.9	191.7	4.7	-81.2	-158.2	33.5	-76.5
	Rb ⁺	-34.8	187.6	5.1	-67.6	-159.9	27.7	-62.5
	Li ⁺	-23.8	330.1	9.9	-132.7	-231.1	99.0	-122.8
	Na ⁺	-37.0	304.1	9.6	-118.0	-232.6	71.5	-108.4
	K ⁺	-39.2	286.4	5.1	-96.9	-233.7	52.7	-91.8
GQ-K ⁺ -M ⁺	Rb ⁺	-32.9	282.2	4.4	-85.0	-234.5	47.7	-80.7

^a All energies were computed with the DFT-D method at the ZORA-BLYP-D3(BJ)/TZP(DZ) level of theory.



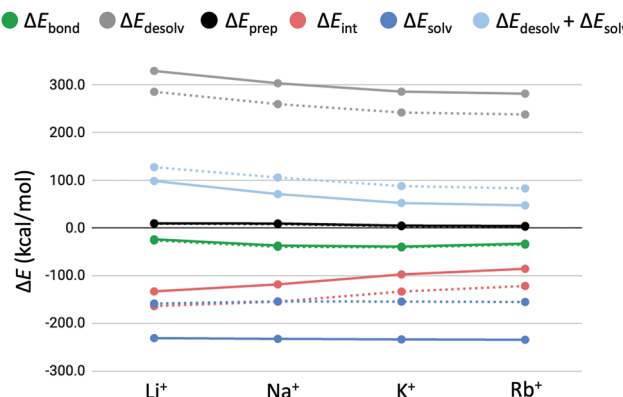


Fig. 5 Partitioning of the bond energy (in kcal mol^{-1}) between the alkali metal cations (M^+) and $\text{GQ}-[\]$ (dashed lines) and $\text{GQ}-\text{K}^+-[\]$ (solid lines).

The former combination follows almost the exact same trend as the interaction energy alone. Table 3 shows that both summations are of counteracting and almost of equal importance to the order of cation affinity, resulting in small differences in bonding energy for the different alkali cations. The results of the double-layer GQs in Table 3 are consistent with the results found by Zaccaria *et al.*²³ With this we would like to emphasize that the improved COSMO version results in different absolute energies, but yields the same relative energies and trends. The trends of the bond energy and the partitions are the same for both the double and triple-layer quadruplexes (Fig. 5). Remarkably, the magnitude of the bond energy decreases only little, going from the first to the second binding event. That the overall bond energy stays approximately the same for the first and second binding event of alkali metal cations of the same kind is the result of two counteracting effects: (1) the interaction energy (ΔE_{int}) is less stabilizing for the interaction of the second metal cation (M^+) with the cavity of the GQ than for the first metal cation; (2) the sum of solvation effects ($\Delta E_{\text{desolv}} + \Delta E_{\text{solv}}$) is less destabilizing for the second binding event. The latter is because the stabilizing ΔE_{solv} term increases more than the destabilizing ΔE_{desolv} term, going from the first to the second binding cation. In other words, the gain in solvation energy (ΔE_{solv}) for going from a GQ of charge 1^+ ($\text{GQ}-\text{M}^+$) to 2^+ ($\text{GQ}-\text{K}^+-\text{M}^+$) is larger, than the increase of desolvation energy (ΔE_{desolv}) for going from a neutral GQ ($\text{GQ}-[\]$) to a positively charged species ($\text{GQ}-\text{K}^+-[\]$). This can be explained by the fact that in the 2^+ species the charge is more localized, resulting in more polarization of the solvent and thereupon to stronger interactions than in the case of 1^+ species. It must be examined if this effect will be even stronger in highly charged systems (3^+ , 4^+ , etc.).

3.4 Energy decomposition analysis

The previous section showed that the desolvation energy and the size of the cation contribute equally to the bond energy of the alkali metal cations in the double and triple-layer guanine quadruplexes. The bond energy stays equal for binding a second metal cation, although a less stabilizing interaction

energy was observed going from the double to the triple-layer quadruplexes. In order to get a better understanding of the reason why the interaction energy is less stabilizing for the second binding event, ΔE_{int} is decomposed into physically meaningful terms (see eqn (7), Table 4 and Fig. 6). The interaction energy terms follow the same trend for both the guanine quadruplexes with and without sugar-phosphate backbone. The results of the systems with sugar-phosphate backbone (GQ) are graphically presented in Fig. 6.

From Fig. 6, it can be seen that the significant drop in interaction energy going from Na^+ to K^+ is due to the increase in Pauli repulsion that increases by almost 20 kcal mol^{-1} . We want to emphasize this counterintuitive observation that K^+ results in less deformation of the GQ, although it is accompanied by a higher Pauli repulsion than Na^+ . From the energy decomposition analysis (EDA) follows that the bonding interaction of the second alkali cation to $\text{GQ}-\text{K}^+-[\]$ is a combination of mainly electrostatic interaction, followed by orbital interaction and dispersion. These trends are also in line with the results found by Zaccaria *et al.*²³ In fact, the trendlines of the energy terms ΔE_{Pauli} , ΔE_{oi} and ΔE_{disp} do exactly overlap for the double- and triple-layered GQs. It turns out that only the decrease in electrostatic interaction (ΔV_{elstat}) is responsible for the observed decrease in interaction energy in the second binding event.

The observed decrease in electrostatic interaction (ΔV_{elstat}) for binding of the second alkali cation can be the result of the repulsion between the two present cations in the quadruplex or the diminished electron density available on middle guanine quartet to bind the second cation. The presence of the first potassium ion in $\text{GQ}-\text{K}^+-[\]$ leads to extraction of electron density from the oxygen atoms. Thereupon, the oxygen atoms in the middle guanine quartet layer of $\text{GQ}-\text{K}^+-\text{M}^+$ are likely to become less electronegative, potentially leading

Table 4 Partitioning of the interaction energy (in kcal mol^{-1}) of alkali metal cations (M^+) with $\text{G}_4-[\]-\text{G}_4$, $\text{GQ}-[\]$, $\text{G}_4-\text{K}^+-\text{G}_4-[\]-\text{G}_4$ and $\text{GQ}-\text{K}^+-[\]$ ^a

System	M^+	ΔE_{int}	ΔV_{elstat}	ΔE_{Pauli}	ΔE_{oi}	ΔE_{disp}
$\text{G}_4-\text{M}^+-\text{G}_4$	Li^+	-159.4	-108.2	11.6	-54.8	-8.0
	Na^+	-150.0	-105.3	11.2	-43.0	-12.9
	K^+	-127.2	-102.1	30.9	-40.8	-15.2
	Rb^+	-114.3	-96.0	36.6	-38.4	-16.5
$\text{GQ}-\text{M}^+$	Li^+	-163.6	-111.0	12.9	-58.0	-7.4
	Na^+	-154.2	-106.8	10.3	-44.6	-13.1
	K^+	-133.1	-103.6	28.4	-42.3	-15.6
	Rb^+	-121.5	-99.2	34.8	-40.1	-16.9
$\text{G}_4-\text{K}^+-\text{G}_4-\text{M}^+-\text{G}_4$	Li^+	-119.1	-66.0	11.7	-56.1	-8.7
	Na^+	-105.2	-56.8	11.8	-45.3	-14.9
	K^+	-81.3	-51.3	30.9	-42.7	-18.2
	Rb^+	-68.2	-46.7	37.1	-40.3	-18.2
$\text{GQ}-\text{K}^+-\text{M}^+$	Li^+	-132.7	-78.6	11.8	-57.9	-8.0
	Na^+	-118.0	-66.7	10.1	-46.4	-15.0
	K^+	-96.9	-62.1	27.4	-43.7	-18.5
	Rb^+	-84.9	-57.6	33.4	-41.6	-19.1

^a All energies were computed with the DFT-D method at the ZORA-BLYP-D3(BJ)/TZP (G_4) or at the ZORA-BLYP-D3(BJ)/TZP/DZ (GQ) level of theory.

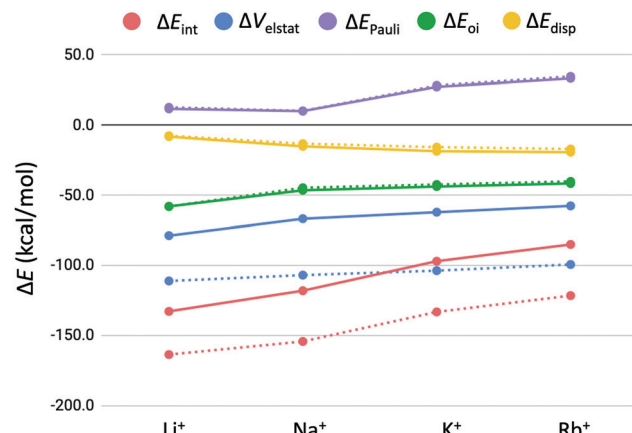


Fig. 6 Energy decomposition of the interaction energy (in kcal mol^{-1}) between the alkali metal cations (M^+) and $\text{GQ}-[\]$ (dashed lines) and $\text{GQ}-\text{K}^+-[\]$ (solid lines).

to less stabilizing electrostatic interaction with the second alkali cation M^+ .

In order to identify the effect of electron depletion of the middle guanine stack upon binding of the first alkali cation, it was examined whether there is diminished charge-transfer from the guanine bases to the second metal cation. Therefore, the VDD change in atomic charge to the second metal cation (ΔQ_{M^+}) was calculated for the triple-layer GQs and compared to the values found for the two-layer GQs (eqn (8) and Table 5). As presented in Table 5, the charge-transfer interaction between the GQ and the second cation is equal to the values found for binding of the first alkali cation in two-layer GQ. This indicates that there is sufficient electron density left on the middle guanine quartet to donate the same number of electrons to the second cation. This observation is supported by the overlapping of ΔE_{oi} (green lines in Fig. 6) for the binding of the first and second cation in the double-layer and triple-layer GQ systems, respectively.

To investigate the contribution of repulsive interactions as cause of the diminished electrostatic interaction, an EDA of the interaction energy between the two alkali cations in $\text{GQ}-\text{K}^+-\text{M}^+$ was performed at the inter-atomic distance within the GQ (see Table 6). The results demonstrate that a large destabilizing interaction is present between the alkali cations in the quadruplex with interaction energies of *ca.* +80 kcal mol^{-1} . Table 6 shows that this destabilizing interaction is almost exclusively due to repulsive electrostatic interactions between the two

Table 5 VDD change in atomic charge (ΔQ_{M^+} , in electrons) to the alkali metal cation in the triple and double layer quadruplexes^a

M^+	$\Delta Q_{\text{M}^+} (\text{GQ}-\text{K}^+-\text{M}^+)$	$\Delta Q_{\text{M}^+} (\text{GQ}-\text{M}^+)$ ²³
Li ⁺	-0.146	-0.142
Na ⁺	-0.085	-0.079
K ⁺	-0.059	-0.058
Rb ⁺	-0.054	-0.054

^a VDD charges were computed with the DFT-D method at the ZORA-BLYP-D3(BJ)/TZP/DZ level of theory.

cations. The electrostatic interaction is less stabilizing by approximately +40 kcal mol^{-1} (ΔV_{elstat}) for all the different cations in $\text{GQ}-\text{K}^+-\text{M}^+$ compared to the two-layered quadruplexes (see difference in ΔV_{elstat} in Fig. 6 for the triple-layer (solid line) and double-layer GQ (dashed line)). Therefore, it is expected that the large repulsive interaction energy between the two alkali cations contributes significantly to the observed decrease in bond energy of the second alkali metal cation but is reduced by electronic shielding of the guanine bases.

Note that the trend in electrostatic repulsion among the different alkali metal cations is related to the distance between K^+ and the second alkali metal cation in the geometry of $\text{GQ}-\text{K}^+-\text{M}^+$ ($d[\text{K}^+-\text{M}^+]$ in Table 6).

It can be concluded that the strong repulsive interaction between the two alkali metal cations, as found by the results in Table 6, accounts for the decrease in interaction energy of the second binding event in guanine quadruplex systems, rather than electron depletion of the middle guanine layer. This would suggest that in even larger multi-layer guanine quadruplexes, where each cation is adjacent to two other cations, the interaction energy for hosting alkali cations would decrease even further. These results question the role of alkali metal cations in the stabilization of multi-layer guanine quadruplex DNA and whether each cavity hosts an alkali metal cation or that rather an alternating pattern of empty and occupied is preferred. The decreasing importance of the alkali metal cations for the stability of multi-layer quadruplexes is in line with the results find by Kotlyar *et al.*⁵³ In this work they report G_4 DNA wires in the absence of alkali cations that show equal stability as the cation containing G_4 structures reported in literature. The high stability is probably the result of the much greater length of these structures.

3.5 Four-layer guanine quadruplexes

In order to see if the interaction energy for binding a third K^+ ion would decrease even further, a four-layer GQ without sugar-phosphate backbone hosting three K^+ ions was examined ($\text{G}_4-\text{K}^+-\text{G}_4-\text{K}^+-\text{G}_4-\text{K}^+-\text{G}_4$). The usage of quadruplexes without sugar-phosphate backbone was justified by the previous results of this work. The bond energy (ΔE_{bond}) of the third K^+ ion was partitioned into different terms in the same way as was done for the triple-layer and double-layer systems (Fig. 7). It was found

Table 6 Energy decomposition analysis (in kcal mol^{-1}) of the interaction between the two alkali cations in $\text{GQ}-\text{K}^+-\text{M}^+$ ^a

M^+	ΔE_{int}	ΔV_{elstat}	ΔE_{Pauli}	ΔE_{oi}	ΔE_{disp}	$\Delta \Delta V_{elstat}^b$	$d[\text{K}^+-\text{M}^+]$
Li ⁺	61.8	68.5	0.0	-0.3	-6.4	34.2	48.5
Na ⁺	88.1	90.2	0.0	-0.9	-1.2	42.6	36.8
K ⁺	86.2	88.7	0.1	-1.5	-1.2	44.2	37.5
Rb ⁺	83.4	86.1	0.2	-1.7	-1.1	39.5	38.5

^a All energies were computed with the DFT-D method at the ZORA-BLYP-D3(BJ)/TZP(DZ) level of theory. ^b Difference in the electrostatic interaction component of the bond energy of $\text{GQ}-\text{K}^+-\text{M}^+$ vs. the two-layer $\text{GQ}-\text{M}^+$ of Zaccaria *et al.*²³ (see Fig. 6). ^c Distance (in Å) between K^+ and the second alkali metal cation in $\text{GQ}-\text{K}^+-\text{M}^+$.



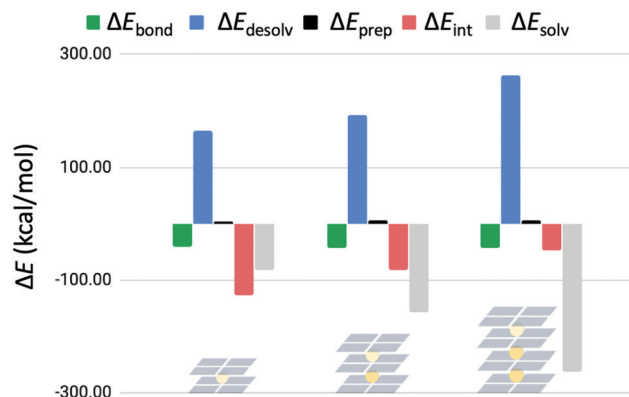


Fig. 7 Partitioning of the bond energy (in kcal mol^{-1}) for subsequent binding events of K^+ in $\text{G}_4\text{-K}^+\text{-G}_4$, $\text{G}_4\text{-K}^+\text{-G}_4\text{-K}^+\text{-G}_4$ and $\text{G}_4\text{-K}^+\text{-G}_4\text{-K}^+\text{-G}_4\text{-K}^+\text{-G}_4$.

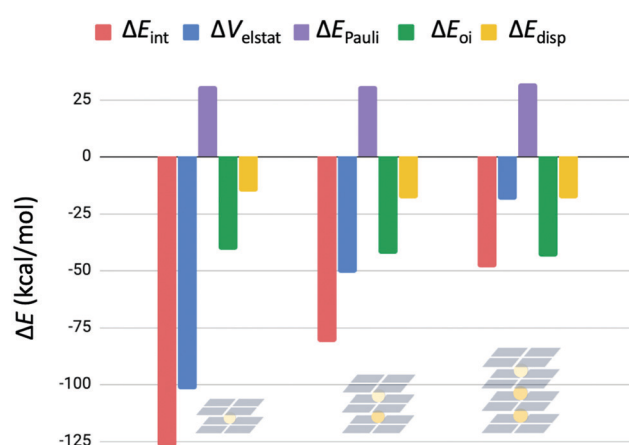


Fig. 8 Energy decomposition of the interaction energy (in kcal mol^{-1}) for subsequent binding events of K^+ in $\text{G}_4\text{-K}^+\text{-G}_4$, $\text{G}_4\text{-K}^+\text{-G}_4\text{-K}^+\text{-G}_4$ and $\text{G}_4\text{-K}^+\text{-G}_4\text{-K}^+\text{-G}_4\text{-K}^+\text{-G}_4$.

again that the bond energy stays approximately equal for binding of the third cation.

In Fig. 7 the preparation energy stays the same, but the interaction energy decreases for each binding event. In addition, the contribution of solvation effects becomes more significant following this trend. The stabilizing solvation energy increases faster than the destabilizing desolvation energy with each binding event, resulting in an equalized bond energy.

The interaction energy is further decomposed into physically meaningful terms for consecutive binding events in $\text{G}_4\text{-K}^+\text{-G}_4$, $\text{G}_4\text{-K}^+\text{-G}_4\text{-K}^+\text{-G}_4$ and $\text{G}_4\text{-K}^+\text{-G}_4\text{-K}^+\text{-G}_4\text{-K}^+\text{-G}_4$ (see eqn (7) and Fig. 8). Fig. 8 shows that the energy terms ΔE_{Pauli} , ΔE_{oi} and ΔE_{disp} stay the same for the subsequent binding events of K^+ in double- and triple- and four-layer quadruplexes. It is only the decrease in electrostatic interaction (ΔV_{elstat}) that is responsible for the observed decrease in interaction energy in sequel binding events. These results show that electrostatic repulsion operates not only locally, but operates also over long range distances.

4. Conclusions

Alkali metal cations are found to stabilize the assembly of guanine quadruplexes in nature. In this work, the alkali metal cation affinity of double-, triple- and four-layer guanine quadruplexes was studied using dispersion-corrected density functional theory (DFT-D). The computational results show an increasing stabilizing interaction of the order $\text{Li}^+ < \text{Rb}^+ < \text{Na}^+ < \text{K}^+$ for the double and triple-layer quadruplexes, which is in agreement with the experimental order of affinity.

Partitioning of the bond energy between the alkali cation and the cavity of the quadruplexes, showed that the desolvation energy and the size of the cation are of equal importance to the trend. Descending the first group of the periodic table shows a decrease of the desolvation energy of the cation, and a decrease of the attractive interaction between the cation and the quadruplex. Simultaneously, hosting of the larger cations diminishes the deformation of the empty quadruplex cavity. These effects result together in a minimum of the bond energy for K^+ .

The magnitude of the bond energy stays approximately the same for the subsequent binding events of a first, second and third cation in double, triple and four-layer guanine quadruplexes, respectively. Although the interaction energy decreases for each binding event, the contribution of solvation effects becomes more significant following this trend. The stabilizing solvation energy increases faster than the destabilizing desolvation energy with each binding event, resulting in an equalized bond energy.

Decomposition of the interaction energy into physically meaningful terms showed that electrostatic repulsion between the hosted metal cations is responsible for the diminished interaction energy. This work demonstrates that solvent effects become of increasing importance for the stabilization of highly charged multi-layer guanine quadruplex DNA.

Conflicts of interest

There are no conflicts to declare.

Acknowledgements

C. F. G. gratefully acknowledges the financial support from the Netherlands Organization for Scientific Research NWO (ECHO).

References

1. S. Neidle and S. Balasubramanian, *Quadruplex Nucleic Acids*, Royal Society of Chemistry, Cambridge, 2006.
2. M. L. Bochman, K. Paeschke and V. A. Zakian, *Nat. Rev. Genet.*, 2012, **13**, 770–780.
3. R. Hänsel-Hertsch, M. Di Antonio and S. Balasubramanian, *Nat. Rev. Mol. Cell Biol.*, 2017, **18**, 279–284.
4. J. T. Davis, *Angew. Chem., Int. Ed.*, 2004, **43**, 668–698.
5. E. Henderson, C. C. Hardin, S. K. Walk, I. Tinoco and E. H. Blackburn, *Cell*, 1987, **51**, 899–908.



- 6 G. Biffi, M. Di Antonio, D. Tannahill and S. Balasubramanian, *Nat. Chem.*, 2014, **6**, 75–80.
- 7 S. Ray, J. N. Bandaria, M. H. Qureshi, A. Yildiz and H. Balci, *Proc. Natl. Acad. Sci. U. S. A.*, 2014, **11**, 2990–2995.
- 8 S. Neidle, *Therapeutic Applications of Quadruplex Nucleic Acids*, Elsevier Academic Press, 2012.
- 9 L. Stefan and D. Monchaud, *Nat. Rev. Chem.*, 2019, **3**, 650–668.
- 10 S. Balasubramanian and S. Neidle, *Curr. Opin. Chem. Biol.*, 2009, **13**, 345–353.
- 11 A. R. Duarte, E. Cadoni, A. S. Ressurreição, R. Moreira and A. Paulo, *ChemMedChem*, 2018, **13**, 869–893.
- 12 Q. Cao, Y. Li, E. Freisinger, P. Z. Qin, R. K. O. Sigel and Z. Mao, *Inorg. Chem. Front.*, 2017, **4**, 10–32.
- 13 C. Fonseca Guerra, H. Zijlstra, G. Paragi and F. M. Bickelhaupt, *Chem. – Eur. J.*, 2011, **17**, 12612–12622.
- 14 L. P. Wolters, N. W. G. Smits and C. Fonseca Guerra, *Phys. Chem. Chem. Phys.*, 2015, **17**, 1585–1592.
- 15 L. Guillaumes, S. Simon and C. Fonseca Guerra, *ChemistryOpen*, 2015, **4**, 318–327.
- 16 J. Poater, M. Swart, F. M. Bickelhaupt and C. Fonseca Guerra, *Org. Biomol. Chem.*, 2014, **12**, 4691–4700.
- 17 C. Fonseca Guerra, F. M. Bickelhaupt and E. J. Baerends, *ChemPhysChem*, 2004, **5**, 481–487.
- 18 C. Fonseca Guerra, Z. Szekeres and F. M. Bickelhaupt, *Chem. – Eur. J.*, 2011, **17**, 8816–8818.
- 19 P. Gilli, V. Bertolasi, V. Ferretti and G. Gilli, *J. Am. Chem. Soc.*, 2000, **122**, 10405–10417.
- 20 J. R. Williamson, *Annu. Rev. Biophys. Biomol. Struct.*, 1994, **23**, 703–730.
- 21 J. Gu, J. Leszczynski and M. Bansal, *Chem. Phys. Lett.*, 1999, **311**, 209–214.
- 22 Z. Wang and J. P. Liu, *Clin. Exp. Pharmacol. Physiol.*, 2015, **42**, 902–909.
- 23 F. Zaccaria, G. Paragi and C. Fonseca Guerra, *Phys. Chem. Chem. Phys.*, 2016, **18**, 20895–20904.
- 24 F. Zaccaria and C. Fonseca Guerra, *Chem. – Eur. J.*, 2018, **24**, 16315–16322.
- 25 R. Ida and G. Wu, *J. Am. Chem. Soc.*, 2008, **130**, 3590–3602.
- 26 C. Detellier and P. Laszlo, *J. Am. Chem. Soc.*, 1980, **102**, 1135–1141.
- 27 A. Wong and G. Wu, *J. Am. Chem. Soc.*, 2003, **125**, 13895–13905.
- 28 J. R. Williamson, M. K. Raghuraman and T. R. Cech, *Cell*, 1989, **59**, 871–880.
- 29 J. Gu and J. Leszczynski, *J. Phys. Chem. A*, 2002, **106**, 529–532.
- 30 N. V. Hud, F. W. Smith, F. A. L. Anet and J. Feigon, *Biochemistry*, 1996, **35**, 15383–15390.
- 31 S. Grimme, J. Antony, S. Ehrlich and H. Krieg, *J. Chem. Phys.*, 2010, **132**, 154104.
- 32 S. Grimme, S. Ehrlich and L. Goerigk, *J. Comput. Chem.*, 2011, **32**, 1456–1465.
- 33 S. Grimme, *J. Comput. Chem.*, 2004, **25**, 1463–1473.
- 34 S. Grimme, *J. Comput. Chem.*, 2006, **27**, 1787–1799.
- 35 C. Fonseca Guerra, T. van der Wijst, J. Poater, M. Swart and F. M. Bickelhaupt, *Theor. Chem. Acc.*, 2010, **125**, 245–252.
- 36 T. van der Wijst, C. Fonseca Guerra, M. Swart, F. M. Bickelhaupt and B. Lippert, *Angew. Chem., Int. Ed.*, 2009, **48**, 3285–3287.
- 37 G. N. Parkinson, M. P. H. Lee and S. Neidle, *Nature*, 2002, **417**, 876–880.
- 38 G. te Velde, F. M. Bickelhaupt, E. J. Baerends, C. Fonseca Guerra, S. J. A. van Gisbergen, J. G. Snijders and T. Ziegler, *J. Comput. Chem.*, 2001, **22**, 931–967.
- 39 C. Fonseca Guerra, J. G. Snijders, G. te Velde and E. J. Baerends, *Theor. Chem. Acc.*, 1998, **99**, 391–403.
- 40 E. J. Baerends, *et al.*, ADF2017.103, SCM, Theoretical Chemistry, Vrije Universiteit, Amsterdam, The Netherlands <http://www.scm.com>.
- 41 E. van Lenthe, A. Ehlers and E. J. Baerends, *J. Chem. Phys.*, 1999, **110**, 8943–8953.
- 42 J. Šponer, A. Mládek, N. Špačková, X. Cang, T. E. Cheatham, III and S. Grimme, *J. Am. Chem. Soc.*, 2013, **135**, 9785–9796.
- 43 R. Sedlak, T. Janowski, M. Pitoňák, J. Řezáč, P. Pulay and P. Hobza, *J. Chem. Theory Comput.*, 2013, **9**, 3364–3374.
- 44 A. Klamt and G. Schüürmann, *J. Chem. Soc., Perkin Trans. 2*, 1993, 799–805.
- 45 A. Klamt, *J. Phys. Chem.*, 1995, **99**, 2224–2235.
- 46 C. C. Pye, T. Ziegler, E. van Lenthe and J. N. Louwen, *Can. J. Chem.*, 2009, **87**, 790–797.
- 47 F. M. Bickelhaupt and E. J. Baerends, *Rev. Comput. Chem.*, 2002, **15**, 1–86.
- 48 C. Fonseca Guerra, J. W. Handgraaf, E. J. Baerends and F. M. Bickelhaupt, *J. Comput. Chem.*, 2004, **25**, 189–210.
- 49 O. A. Stasyuk, H. Szatylowicz, T. M. Krygowski and C. Fonseca Guerra, *Phys. Chem. Chem. Phys.*, 2016, **18**, 11624–11633.
- 50 C. Fonseca Guerra, F. M. Bickelhaupt, J. G. Snijders and E. J. Baerends, *J. Am. Chem. Soc.*, 2000, **122**, 4117–4128.
- 51 C. Fonseca Guerra, F. M. Bickelhaupt, J. G. Snijders and E. J. Baerends, *Chem. – Eur. J.*, 1999, **5**, 3581–3594.
- 52 T. J. Pinnavaia, C. L. Marshall, C. M. Mettler, C. L. Fisk, H. T. Miles and E. D. Becker, *J. Am. Chem. Soc.*, 1978, **100**, 3625–3627.
- 53 A. B. Kotlyar, N. Borovok, T. Molotsky, H. Cohen, E. Shapir and D. Porath, *Adv. Mater.*, 2005, **17**, 1901–1905.

